ARTICLE

Experimental study of moment redistribution before yielding in precast prestressed concrete beams made continuous

Ulla Kytölä [ORCID] | Joonas Tulonen [ORCID] | Olli Asp [ORCID] | Tarja Nakari |
Anssi Laaksonen [ORCID]

Faculty of Built Environment—Concrete and Bridge Structures, Tampere University, Tampere, Finland

Correspondence
Ulla Kytölä, Faculty of Built Environment—Concrete and Bridge Structures, Tampere University, Tampere, Finland.
Email: ulla.kytola@tuni.fi

Funding information
Finnish Concrete Industry

Abstract

The bending stiffness distribution of beams composed of simple-span precast prestressed beams, which are made continuous by deck reinforcement at intermediate supports, is not constant. As the structure undergoes loading, the deck slab at the intermediate support cracks earlier than the prestressed span soffit and due to that the bending stiffness distribution changes along the beam length. The effect of nonconstant bending stiffness distribution on the moment redistribution of the structure before the yielding is studied experimentally and analytically. Two continuous beams with spans of 10 m + 10 m were manufactured, loaded to failure, and studied. It was concluded that the studied structure undergoes considerable moment redistribution before yielding although it would be designed for zero redistribution at the ultimate limit state. If this elastic redistribution is neglected in the structural analysis, the service limit state sagging moment at midspan may end up on the unconservative side. Elastic redistribution can be predicted quite accurately with the help of nonlinear analysis or roughly with simplified idealization as proposed in this article.

KEYWORDS
bending stiffness, moment redistribution, moment–curvature, precast concrete, prestressed concrete, statically indeterminate structures

1 | INTRODUCTION

The benefits of making precast, prestressed multi-girders continuous by connecting the simple-span beams with a continuity diaphragm were recognized by researchers and designers already in 1960. Continuity reduces both the maximum moments and deflections at the mid-span of a beam. For continuous beams, longer span lengths or fewer strands may be achieved. The continuity could also help provide robustness in the event of an overload. It is typical to increase the capacity of precast prestressed simple-span bridge beams this way.[1–4]

This article concentrates on precast beams, where continuity connection is provided through tension reinforcement in the in situ cast deck slab over the supports and through compression in the cross beam, which is called a diaphragm. The beams act as simple spans for dead loads before the deck is made continuous over the

center support. After the continuity is obtained, the composite section of the precast girder and deck slab is assumed to bear the superimposed loads as a continuous structure.

The simple-span precast prestressed beam undergoes a time-dependent structural change when it is made continuous after the application of prestress force and self-weight of the structure. Due to this, restraint reactions are produced. Both negative (hogging) and positive (sagging) restraint moments may develop over time to the connections area of the studied structure. If the positive restraint moment is large enough, a gap will open between girder end soffits. One major issue that has dominated the research field and design guidance of this structure type for many years concern the relevance of these positive restraint moments and the loss of continuity because of them.[3,5–10]

So far, however, there has been less discussion about the loss of continuity of the structure due to the cracking of the deck slab at the connection area in the service limit state (SLS). The term "loss of continuity" refers to a drop in hogging moment in the central support compared to the one predicted by elastic theory. This kind of moment redistribution in beams has traditionally been considered an ultimate limit state (ULS) phenomenon closely associated with the consideration of reinforcement ductility and plastic hinge length. Plastic moment redistribution has been a subject of numerous studies and majority of standards have adopted the neutral axis depth factor as a parameter for calculating the limited redistribution in the ULS.[11–20] However, previous research has established that a considerable portion of moment redistribution occurs already at the SLS due to bending stiffness variation, caused by concrete cracking formations. In the literature, this phenomenon is called *elastic redistribution*.[21–25] One reason for the lack of conversation on "elastic redistribution in precast prestressed beams made continuous" may be due to an assumption that during the normal service life of prestressed concrete bridges designed according to specifications, the cracking of the structure is minor. However, this assumption might not be accurate if the studied structure is used for another purpose than bridges, where the limited values for allowable crack widths of concrete are not that tight.

In the design of prestressed concrete structures, the normal practice often is to predict the distribution of bending moments by the elastic theory and the assumption of constant stiffness.[26] The studied structure is special when it comes to its bending stiffness distribution. In the spans, the T-shaped concrete composite beam is prestressed and has a wide compression area at the deck slab toward bending. By contrast in the intermediate support, the continuity connection has only ordinary tension reinforcement, usually lower concrete strength, minor compression flange, and no facilitating prestress force. It is

apparent that bending stiffness distribution of the structure is not constant, and it changes during loading because the cracking of the cross-sections does not coincide. The question is then raised: What is the magnitude of elastic moment redistribution in the precast prestressed beams made continuous?

The purpose of this investigation is to explore the moment redistribution of precast prestressed beams made continuous as load is increased, especially before yielding of continuity reinforcement. Large-scale experimental tests are carried through and the test results are compared to nonlinear analysis. Finally, in this article, an attempt is made to develop a simple approach for determining redistribution of moments at SLS.

2 | EXPERIMENTAL PROGRAM

2.1 | Test beams

In this study, two continuous 20-m-long test beams were fabricated and tested to investigate the behavior of moment redistribution of precast prestressed beams made continuous. The T-shaped specimen consisted of two precast prestressed girders which were connected as a continuous two-spanned beam by a diaphragm and a deck slab.

Exactly, 9875-mm-long, rectangular 280 mm × 480 mm shaped precast beams were cast at the prefabrication factory. The beams were prestressed using 14 seven-wire strands with a diameter of 12.5 mm tensioned to give an initial prestress force of 1200 MPa. All the strands were straight and bonded along the beam length. The prestress force was launched 28 h after the casting of the precast beams. The shear reinforcement of girders consists of bundled spiral stirrups (H2 #8). The composite action between the precast girders and cast-in-place deck was achieved with hairpins (H1, H3) and the rough contact face of the precast girders. The spacing of the stirrups and hairpins (H1, H2, and H3) was tightest near the connection area. Detailed information about precast beams is given in the reinforcement picture of the precast beam in Figure 1. The shear reinforcement of the beams was selected so that shear failure during test shall be avoided.

At the precast beam age of 8 days, two beams, both made up of two separate precast beams, were connected at the Laboratory by a 650-mm-wide crossbeam and a 1100-mm-wide 120-mm-thick deck slab. A short (150-mm-high) column was also cast under the connection area of both beams. The concrete strength class used in the casting of the connection area and deck slab was lower than the one used in the precast girders. The cylinder strengths of the concrete at the time of the loading are presented in Table 1, based on the loading tests of field-cured cylinders (six pcs per batch).
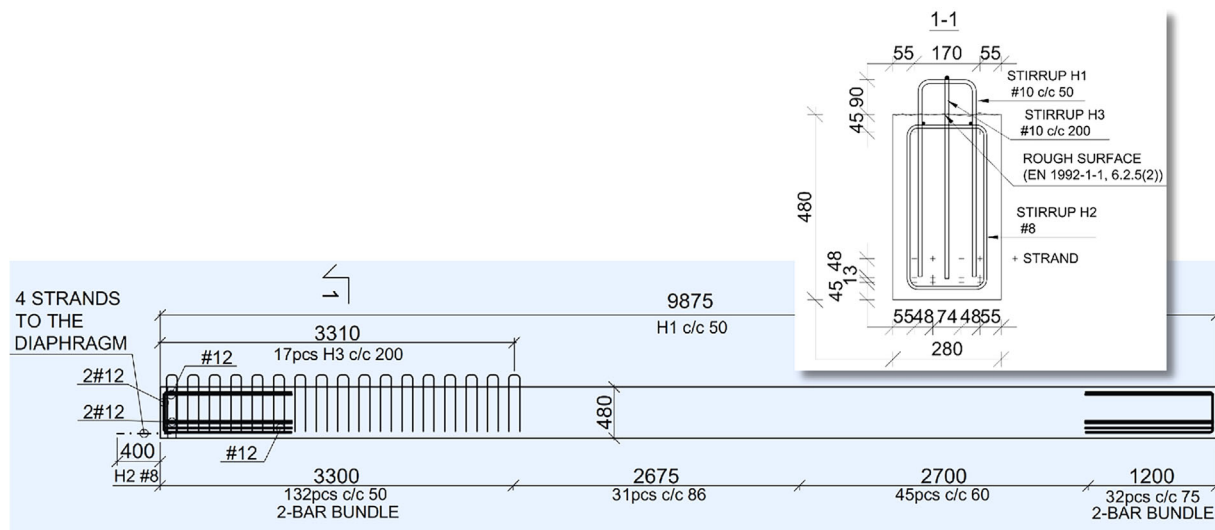
FIGURE 1   Reinforcement of precast prestressed test beams (unit of length in the figure is mm).

TABLE 1   General information about connected beams.

Test beam	Deck slabs ρ_1	ρ_1/ρ_b[a]	Beam age at loading	Slab/diaphragm age at loading	Span $M_{u.calc.span}$ (kNm)	Support $M_{u.calc.sup}$ (kNm)	$M_{u.calc.sup}/M_{u.calc.span}$	Concrete strength f_{cm} (MPa) Beam	Deck slab
B-LIGHT	1.8%	0.55	37 days	29 days	1083[b]	895[c]	0.83	64.2	47.2
B-HEAVY	3.1%	0.96	44 days	36 days	1085[b]	1319[c]	1.22	66.7	48.9

[a]ρ_b is reinforcement ratio at balanced condition calculated according to design strengths.
[b]Calculated according to METHOD 3 determined in Section 4.1.1.
[c]Calculated according to METHOD 2 determined in Section 4.1.1.

The ends of the precast beams were embedded 200 mm into the diaphragm. Four bottom strands were bent into the diaphragm to conduct a positive moment connection. Transverse reinforcement and photographs of the diaphragm are presented in Ref.,[27] where the results of the negative moment capacity of the corresponding connection were studied.

Continuous test specimens weighted 13.4 t each. The girders were lifted out of the formwork of the deck slab and placed on the load cells, that were already measuring the support reactions. Lifting loop locations are presented in the Figure 2. The test beam bears the self-weight of the beam as a continuous structure. Commonly, the precast prestressed beams act as simple spans for their own weight before the deck is made continuous. In this respect, the studied structure behaves slightly differently in the test arrangement than in practice.

Different longitudinal bar reinforcement areas at the continuity connection deck part were selected, on the base of previous research, to study the influence of the support area's bending strength capacity to the moment redistribution. In 1989, Oesterle et al.

recommended to limit reinforcement ratio of the continuity connection to 0.5 times the balanced reinforcement ratio to ensure sufficient ductility at failure in girders of the type investigated in this study.[7] In contrast, the previously conducted experimental tests indicated that the studied structure had ductile failure regardless of reinforcement ratio due to the presence of confinement reinforcement.[27] On the base of these conflicting conclusions, a cross-sectional area of longitudinal continuity reinforcement of the deck slab was selected to be either 2689 mm^2 (0.55ρ_b) or 4700 mm^2 (0.96ρ_b). Transverse reinforcement of the deck slab varied between 283 and 2260 mm^2/m. The beams were coded so that the name of the specimen describes the longitudinal reinforcement degree. B-LIGHT indicates the 2689 mm^2 deck slab reinforcement, while B-HEAVY is the name of the beam with the higher reinforcement amount. The dimensions and reinforcement details of the test beams are shown in Figure 2 and Table 1. The calculated ultimate bending capacities of the mid-span and support sections are also presented. The material properties of prestressing steel and ordinary reinforcement used are presented in Table 2.
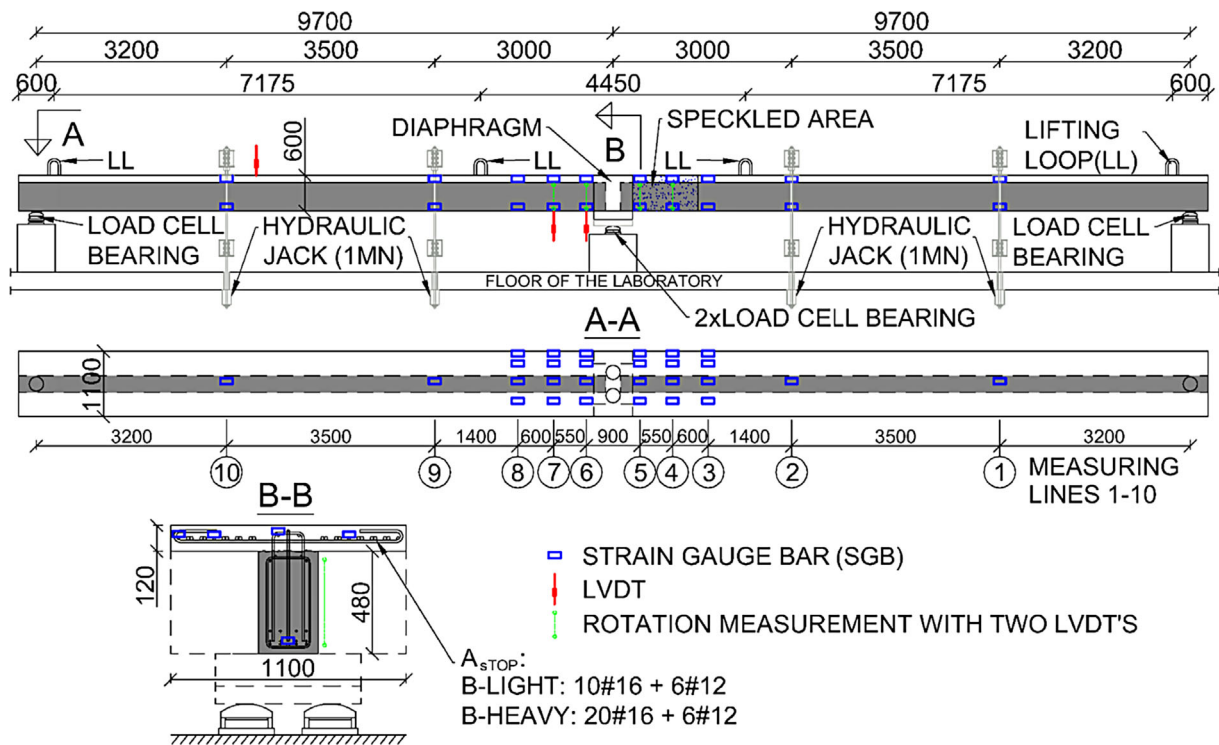
FIGURE 2 Test setup and used instrumentation (unit of length in the figure is mm).

TABLE 2 Reinforcement material properties.

Type of reinforcement	Modulus of elasticity E_s (GPa)	Yield strength f_y or $f_{pk0.1k}$ (MPa)	Area (mm²)	Tensile strength/ upper yield strength R_m/R_{eH}	Elongation at maximum force A_{gt} (%)
B500B T12	200	543–584[a]	112.2–113[a]	1.14–1.17[a]	8–11.2[a]
B500B T16	200	535	200.2	1.22	10.5
Y1860S7-12.5	202.2	1834	91.7	1.0999	5.8

[a]The properties of B500B T12 reinforcement bars variate because the bars came from six different heats.

FIGURE 3 Test setup photographed with fisheye lens.

2.2 | Test setup

The girder is seen under the test in Figure 3. Four-point loads were applied by force-controlled 1 MN hydraulic jacks located below the test floor. The forces of the jacks acted on the girder through pull rods and steel frames. The loading scheme was selected so that its moment distribution would be as similar as possible with the distribution of uniform loading. The applied loads were synchronized to work together to maintain equal value throughout the loading. Because of the inaccuracy in the loading control there was a difference of 0.5–10 kN in the applied loads. The difference was nearly constant throughout the test and its relative value decreased during loading from 7.5% to 2.5% of the point load average.
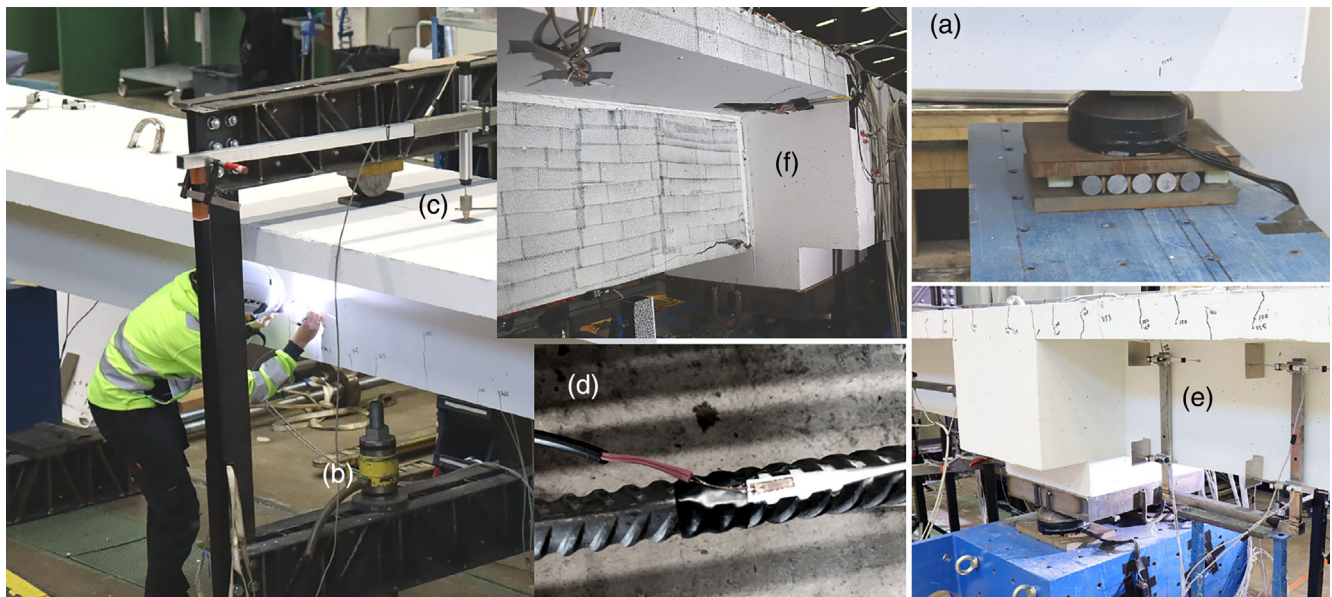
FIGURE 4 Instrumentation of a continuous precast prestressed test girder.

Five load cycles were carried out on both test girders prior to the ultimate loading. In the first four preloading cycles, the load was increased from zero to the service limit state levels SLS1 (two times) and SLS2 (two times) and then returned to zero. SLS1 simulated the quasi-permanent combination of loads, presented in EN 1990, in which decompression of prestressed members with bonded tendons need to be checked according to EN 1992-1-1 regulations.[11,28] The test girders were designed so that they stay in decompression at this load level as simple-span beams without considering the continuity connection. The magnitude of SLS2 was 1.25 times SLS1 and it simulated approximately the frequent combination presented in EN 1990.[28] After the SLS cycles the girders were loaded to failure. The used loading rate was 30 kN/min, and in the final tests, the load steps of 25 kN/jack were used. In total, one test lasted approximately 2 h.

During loading, the following measurements (presented in Figure 4) were made:

a. Reactions at each support using load cells.
b. Load at each loading point using load cells.
c. Deflection using linear variable differential transformers (LVDT's) at measuring lines 6, 7, and 10 (see Figure 2).
d. Tension and compression strain under loading points and hogging moment area using 5-mm strain gages. The gages were attached to the reinforcement bars at measuring lines 1–10 (see Figure 2).
e. The rotation of the beam at measuring lines 4–7 with two horizontal LVDT's located at the side of the web (see Figure 2).

f. Standard DIC techniques use images of the concrete's surface, and strain results of every location of the speckled surface of the specimen are available. The strains of the side of the beam web next to intermediate support were measured with the help of the DIC system. The speckled area of the beam is presented in the Figures 2 and 4.

3 | EXPERIMENTAL RESULTS AND DISCUSSION

3.1 | The degree of moment redistribution at various load levels

In Figure 5, the shape of moment distribution from the loading arrangement in the test setup, at load level where the B-LIGHT failed, is plotted against the beam length. $M_{supLINEAR}$ is the support bending moment calculated using the elastic linear theory while assuming the girders have constant stiffness along their entire length. On the other hand, $M_{supTEST}$ values are the moment distribution during the loading test determined according to the measured support reactions and loads. The bending moment over support is simplified to be constant along the breadth of the support.

The redistribution of moments and observations of the studied structure during the loading test is presented in Figure 6 with the relation between $M_{supTEST}$ and $M_{supLINEAR}$ against the total load applied. Starting point of the analysis is the measured support moment caused by self-weight and loading equipment.
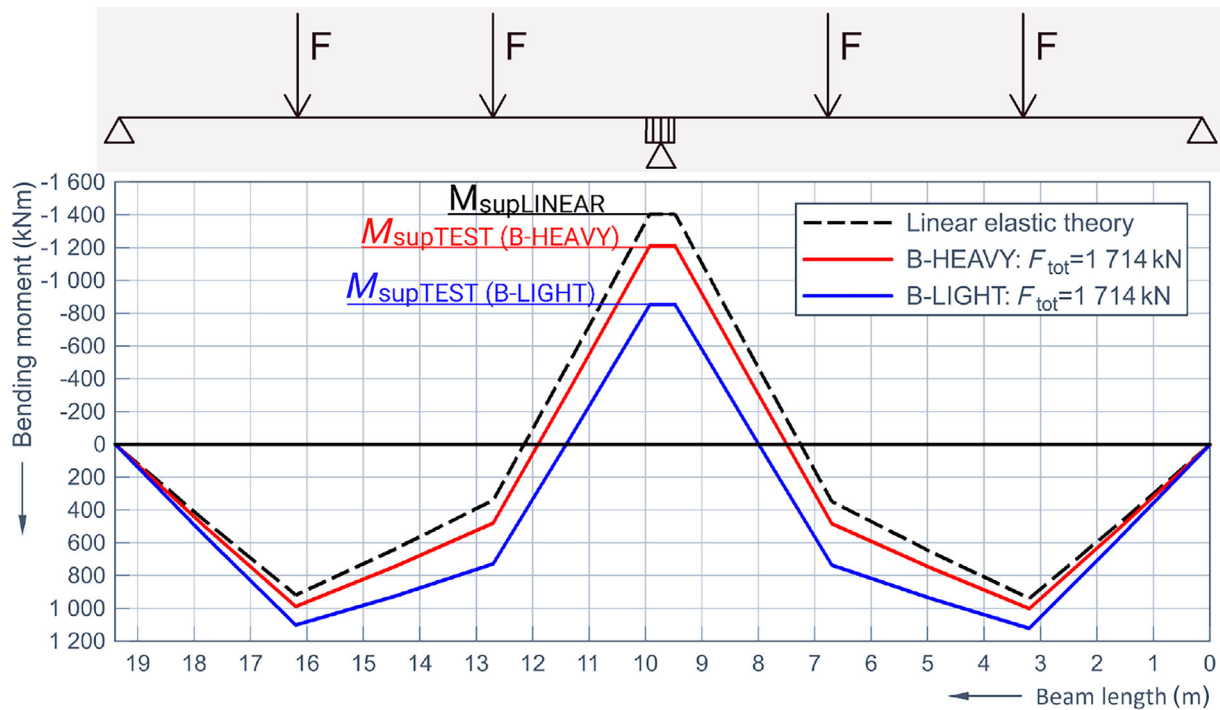
FIGURE 5 Calculated and tested moment distribution diagrams in the test setup.
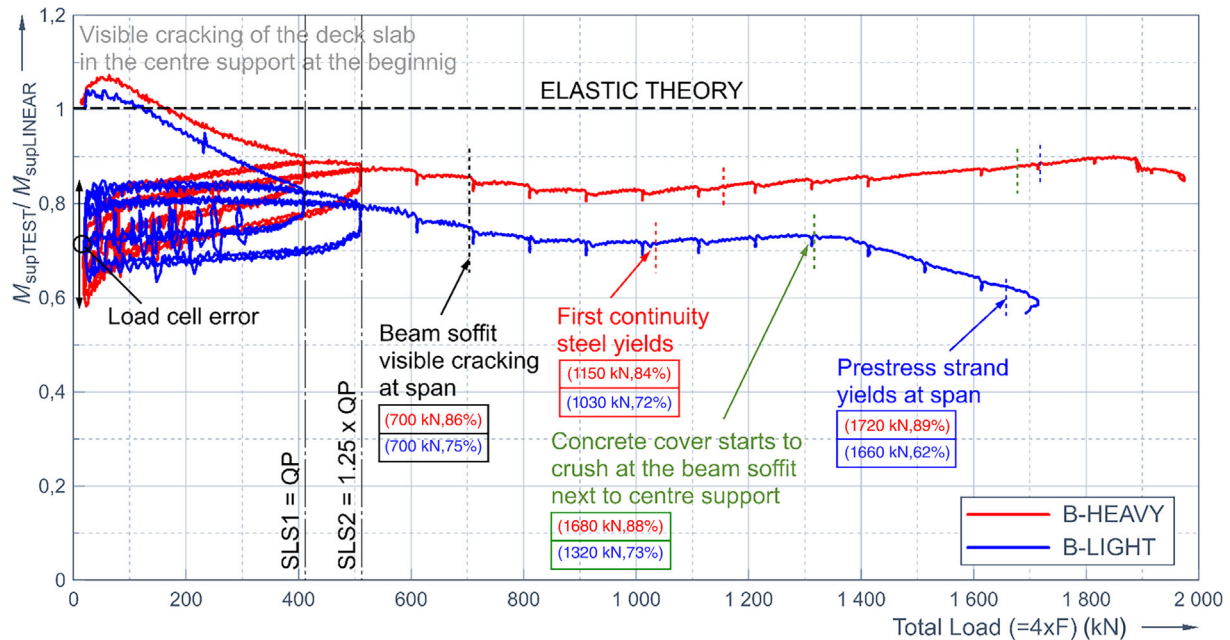

FIGURE 6 Variation of the ratio (Measured center support bending moment = $M_{supTEST}$)/(Calculated center support moment according to linear elastic analysis and the assumption that the stiffness of the girder is constant = $M_{supLINER}$) with increase in total load.

In the beginning of the first SLS1 load step, the degree of continuity was over 100%. The observed over 100% continuity degree in the beginning of the test could be attributed to the tolerances of the experimental arrangement. Minute differences in the altitude of three support levels and unevenness of the bottom of the 20 m long

continuous test beam has probably caused the observed moment redistribution in the beginning of the test.

While the applied load increased above total load level of 100–200 kN support moment began to redistribute to the spans. In the beginning of the second SLS1 step full continuity was no longer achieved. Also the load

reductions of first four SLS1 and SLS2 load step cycles are plotted in Figure 6. $M_{supTEST}/M_{supLINEAR}$ relations is less in the reduction than in the increase of the load. This inconsistency is due to the fact that the accuracy of load cells were not adequate when the load was reduced. The same problem could be observed in the calibration phase of the load cells. After every load reduction, the load was kept at zero load level for 1–4 min before new load increase and due to this the error formed from hysteresis could be eliminated before next load step.

The beam with heavy reinforcement B-HEAVY behaved more similar to linear elastic theory. Nevertheless, before any yielding of continuity reinforcement occurred, support moment of B-HEAVY had dropped for by 16% compared to linear elastic theory. After first yielding B-HEAVY, the bending stiffness of the span decreases more rapidly compared to intermediate support and causes "reverse moment distribution" before failure. The term "First continuity steel yields" presented in Figure 6 refers to a time of loading when the yield limit was exceeded in one of the SGB's located in the deck slab over the web and near the central support (see Figure 2). Simultaneously as the first reinforcement bar yielded over the web the strains of other deck slab reinforcement in the same cross-section remained under the yield limit due to shear lag.

For the B-LIGHT the redistribution of the moments was stronger for the low load levels, and before yielding it had lost its continuity by 28%. After that, the redistribution percentage stayed approximately constant with increasing load until the concrete cover started to spall at beam soffit near the center support. Thereafter ($F_{tot} = 1300$ kN) plastic redistribution began, and total redistribution before failure was 43%.

What stands out from the curves in Figure 6 is that the majority of the redistribution was achieved when the reinforcement was still elastic. For the B-LIGHT, of the 43% total, 28% was elastic redistribution and only 15% was plastic redistribution. Redistribution in the B-HEAVY was higher in the elastic phase than in the actual failure.

According to the results, it is evident that the bending stiffness (EI) of the studied continuous girder changes along the beam length already in low load levels. Cracking of the deck slab reduces the stiffness of the girder region adjacent to the intermediate support and moment begins to redistribute even though all sections along the member are behaving in linearly elastic. This outcome is contrary to AASHTO recommendations which state, that cracking of the concrete has only minor effect to the global behavior of the studied structure and therefore it can be safely neglected by modeling the concrete as uncracked for the purposes of structural analysis.[9]

Mattock and Kaar presented already in 1960 large-scale experimental results which showed similar moment redistribution in the studied structure after the cracking of the deck slab at the support and before the yielding of continuity reinforcement. However, this was not highlighted in the results and conclusions of the study because the studied bridge structure was considered to stay uncracked at designed service load levels.[29] In the next section, the bending stiffness along the beam length of the tested beams is analyzed according to experimental data.

3.2 | EI distribution of tested beams

In Sections 3.2.1 and 3.2.2, the experimentally determined bending stiffness along the beam length is obtained with various methods which use different measurements as an input.

3.2.1 | Simplified EI distribution according to deflection and support reactions

Bending stiffness is an essential factor in determining the deflection of a concrete beam. Although the deflection of the tested beam is measured relatively accurately, it is not a straightforward task to determine the bending stiffness of the indeterminate beam based solely on the deflection and support reaction results. In this study, the problem has been approached from two directions, and the results have been combined (see Figure 7).

In the Option 1, the measured loads (F_1, F_2, F_3, F_4) and support reactions (R_A, R_B, R_C) have been taken advantage of. The unit force method is used to solve moments and reaction forces of the studied indeterminate structure. The center support reactions of the studied two-spanned structure can be determined according to Equation (1),[30,31]

$$R_B = -\frac{\int \dfrac{M_F(x)M_1(x)\,dx}{EI(x)}}{\int \dfrac{M_1(x)M_1(x)\,dx}{EI(x)}} \tag{1}$$

where, $M_F(x)$ is moment at any point in a beam due to applied loads; $M_1(x)$ is moment at any point in a structure due to the unit load at the intermediate support B; $EI(x)$ is the bending stiffness of a member.

If the bending stiffness $EI(x)$ of the beam is constant, it falls out of the equation and has no effect on the support reactions of the continuous beam. The situation is different if $EI(x)$ varies along its length. From the
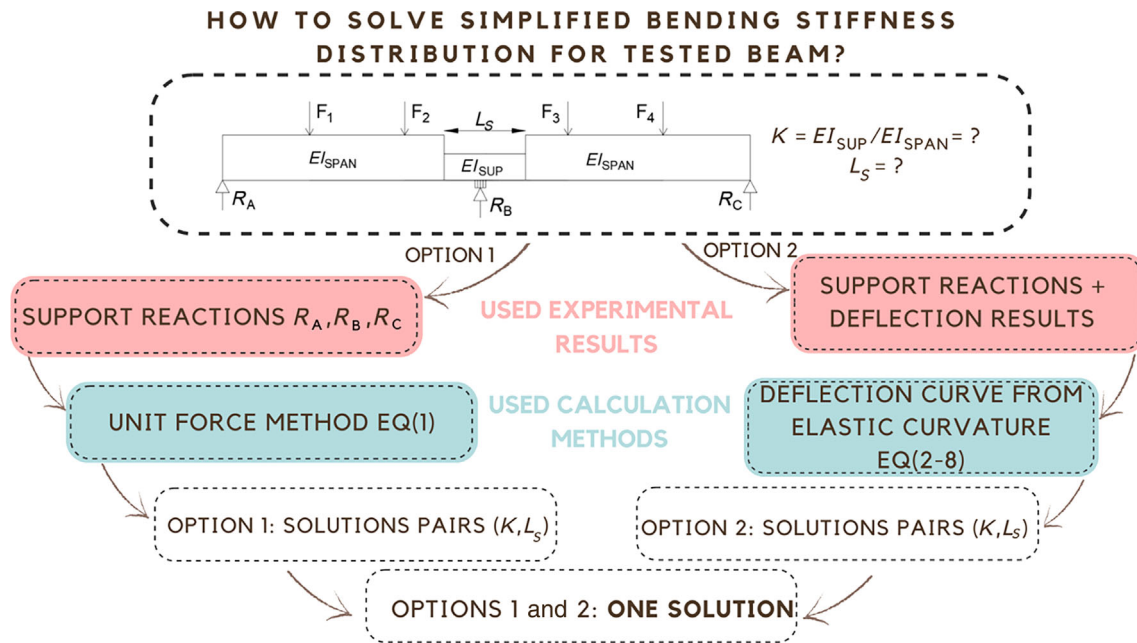
FIGURE 7   Flowchart to explain how to solve simplified bending stiffness distribution from experimental results.

measurements, we can get the load and support reactions during the test. If the structure is simplified to have two constant bending stiffnesses one in the span EI_{SPAN} and one reduced stiffness at center support $EI_{SUPPORT}$ for the selected length L_S (see Figure 7), it is possible to solve the relation K of these two stiffnesses with help of measured support reaction, point loads and Equation 1. The exact values of L_S, EI_{SPAN}, and $EI_{SUPPORT}$ remain unknown variables which cannot be solved when the source information is merely loads and reactions.

In the Option 2, the bending stiffnesses of a simplified nonprismatic continuous beam is solved with the help of measured deflections, loads, and reaction forces. The deflection of a beam can be determined by integrating the differential equation (Equation 2) of the curvature $\kappa(x)$ of a beam twice and using boundary conditions to determine the unknown constants of the integration.[31]

$$v''(x) = \kappa(x) = \frac{M(x)}{EI(x)} \qquad (2)$$

The method is valid as long as cross-sections behave linearly. When solving a deflection of a nonprismatic beam, that is, a beam with nonconstant cross-section, local stress concentrations at the points where the change in cross-section occurs need to be taken into account. The studied beam is symmetrical. Only the deflection of the other span is studied. The studied span is simplified (presented in Figure 8) and cut from its discontinuity point into two segments. The segments are set into balance with the help of equilibrium. The loads and stiffness

of the part with lower EI are multiplied with $1/K$. After this, the segments are connected. A substitute force $(1/K-1)F_p$ and moment $(1/K-1)M_p$ affect the point of discontinuity. Now we have a prismatic beam, with a stiffness of EI/K, and we can get the curvature equation for the entire beam length. The free-body diagrams of the cut segments and final substitute beam are presented in Figure 8.[32]

The elastic deflection curve of the studied span is then,

$$v(x) = \frac{K}{EI}\left(\frac{1}{6}R_A x^3 - \frac{1}{6}F_1\langle x - x_{F1}\rangle^3 - \frac{1}{6}F_2 \qquad (3)\right.$$

$$\langle x - x_{F2}\rangle^3 + \frac{1}{6}F_P\left\langle x - \left(L - \frac{L_S}{2}\right)\right\rangle^3$$

$$\left. - \frac{1}{2}M_P\left\langle x - \left(L - \frac{L_S}{2}\right)\right\rangle^2\right)$$

$$+ \frac{1}{EI}\left(\frac{1}{2}M_P\left\langle x - \left(L - \frac{L_S}{2}\right)\right\rangle^2\right.$$

$$\left. - \frac{1}{6}F_P\left\langle x - \left(L - \frac{L_S}{2}\right)\right\rangle^3\right) + \theta_0 x$$

where, θ_0 is rotation at point x = 0.

From the measurements, we can find R_A, F_1, and F_2. There are four unknowns, K, EI, θ_0, and L_S. From the measurements, we know the deflection of three points
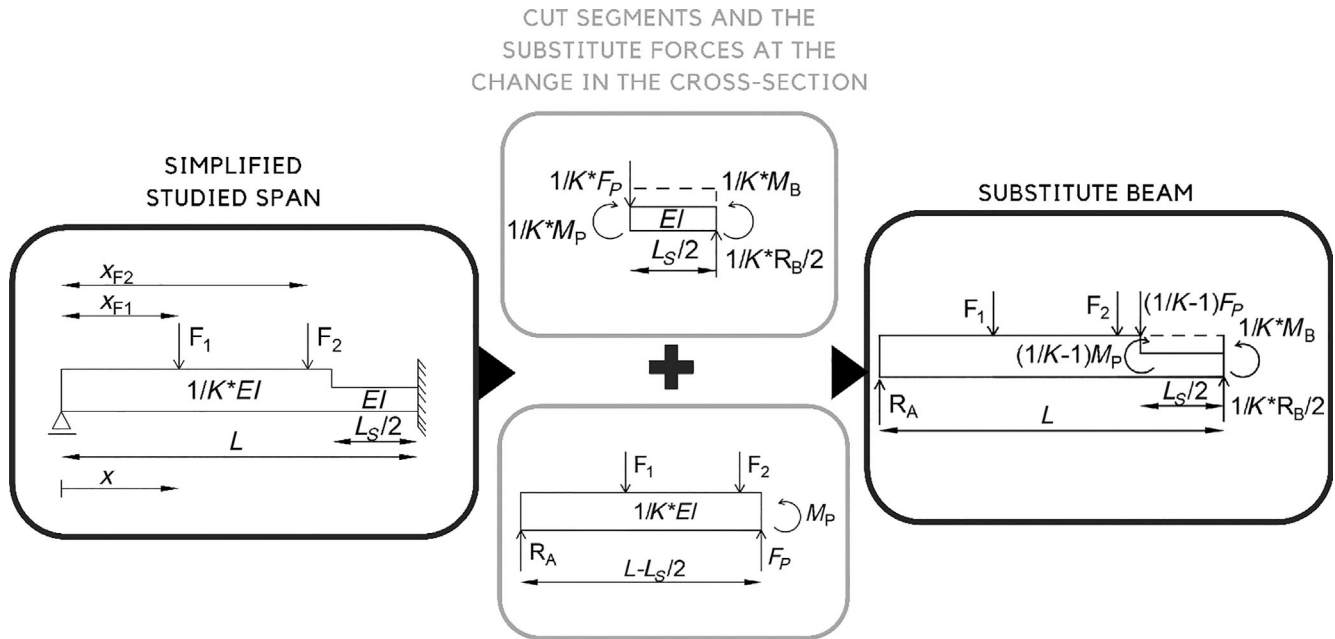
FIGURE 8 Substitute beam for solving the deflection of a two-span continuous nonprismatic beam.

which can be used as boundary conditions, and the system of equations can be solved with the help of the matrix (Equation 4–8). Deflection measurement points 6 and 7 near the center support and from the point of maximum displacement, 10 were selected to describe the shape of the deflection curve.

$$W_1(x) = \frac{1}{6}R_A x^3 - \frac{1}{6}F_1\langle x - x_{F1}\rangle^3 - \frac{1}{6}F_2\langle x - x_{F2}\rangle^3$$
$$+ \frac{1}{6}F_P\left\langle x - \left(L - \frac{L_S}{2}\right)\right\rangle^3$$
$$- \frac{1}{2}M_P\left\langle x - \left(L - \frac{L_S}{2}\right)\right\rangle^2 \quad (4)$$

$$W_2(x) = \frac{1}{2}M_P\left\langle x - \left(L - \frac{L_S}{2}\right)\right\rangle^2 - \frac{1}{6}F_P\left\langle x - \left(L - \frac{L_S}{2}\right)\right\rangle^3 \quad (5)$$

$$W_3(x) = x \quad (6)$$

$$\begin{bmatrix} W_1(x_1) & W_2(x_1) & W_3(x_1) \\ W_1(x_2) & W_2(x_2) & W_3(x_2) \\ W_1(x_3) & W_2(x_3) & W_3(x_3) \end{bmatrix} \cdot \begin{bmatrix} K/EI \\ 1/EI \\ \theta_0 \end{bmatrix} = \begin{bmatrix} v(x_1) \\ v(x_2) \\ v(x_3) \end{bmatrix} \quad (7)$$

$$\begin{bmatrix} K/EI \\ 1/EI \\ \theta_0 \end{bmatrix} = \begin{bmatrix} W_1(x_1) & W_2(x_1) & W_3(x_1) \\ W_1(x_2) & W_2(x_2) & W_3(x_2) \\ W_1(x_3) & W_2(x_3) & W_3(x_3) \end{bmatrix}^{-1} \cdot \begin{bmatrix} v(x_1) \\ v(x_2) \\ v(x_3) \end{bmatrix} \quad (8)$$

Also in this approach, the length of the reduced stiffness L_S remains unknown. The analysis is sensitive at the

low load levels because the deflections near the central support are insignificant in that stage.

The necessary variables K and L_S for the simplified bending stiffness distribution of the test beam are solved by comparing the K ratios calculated according to Options 1 and 2 to each other. A solution pair is found where both these approaches give matching solutions. The ratio of stiffnesses changes constantly during loading, and simultaneously the length of reduced stiffness increases. In the Figure 9, the bending stiffness ratio $K = EI_{\text{SUPPORT}}/EI_{\text{SPAN}}$ is presented during loading for both tested beams and three different L_S values based on Option 1 (based on reactions) and Option 2 (based on reactions and deflections). Load levels before any yielding of reinforcement took place are studied. The range of load level where these two approaches give similar solution for K with $\pm 10\%$ accuracy are highlighted with the colored box. According to the data, we can infer that K stays nearly stable for both test beams in the period under consideration. The values of K vary for B-HEAVY and B-LIGHT at the range of 0.62–0.7 and 0.38–0.44, respectively. By contrast, the lengths of the cracked sector L_S increases as loading proceeds, but after it has reached the value of 0.3 L its increase has only a minor effect on the value of K. In the Table 3 the solutions for four different load levels are summarized.

3.2.2 | Verification of the simplified EI distribution model

The method to verify the simplified bending stiffness distribution of the studied structure is based on the
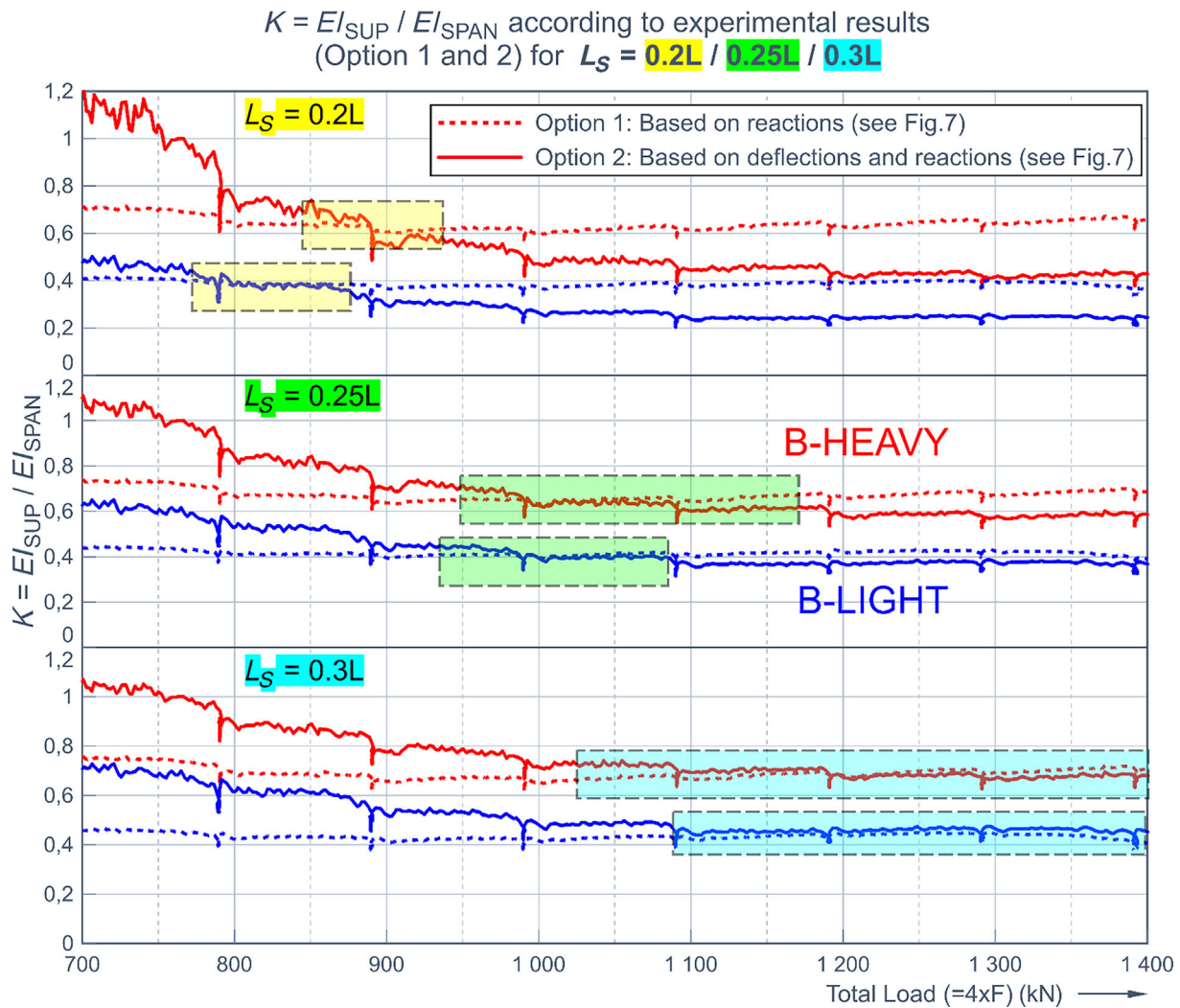
FIGURE 9 Bending stiffness ratio during loading according to the measured support reactions and deflection curve.

Load level (kN)		750–850	850–950	950–1050	1050–1150
B-HEAVY	K	0.62–0.66	0.62–0.63	0.64–0.67	0.68–0.70
	L_S/L	0.14–0.19	0.20–0.22	0.23–0.27	0.28–0.34
B-LIGHT	K	0.38–0.4	0.39–0.41	0.41–0.42	0.43–0.44
	L_S/L	0.19–0.21	0.21–0.24	0.24–0.28	0.29–0.37

TABLE 3 Variables of the simplified bending stiffness model for different load levels.

moment–curvature ($M - \kappa$) relation (Equation 2) and various ways to measure curvature κ of the beam during loading. The curvature of a certain point or distance may be obtained with the help of strain gauge bar, rotation, and DIC measurements. The following briefly describes the methods to determine curvature according to different measurements. Figure 10 provides comparison of EI distribution determined with different methods at load level $F_{tot} = 900$ kN.

EI(x) according to strain gauge measurements
The bottom and top strains at 10 cross-sections of both test beams were measured with SGBs (see Figure 2). Strain gages are one of the most often used tools in strain measurement. Uncertainties of this measuring technique are associated with the unplanned skew of the rather small strain gauge. It is not known does the concrete cracking develop into the same location where the strain gages locate.[33]
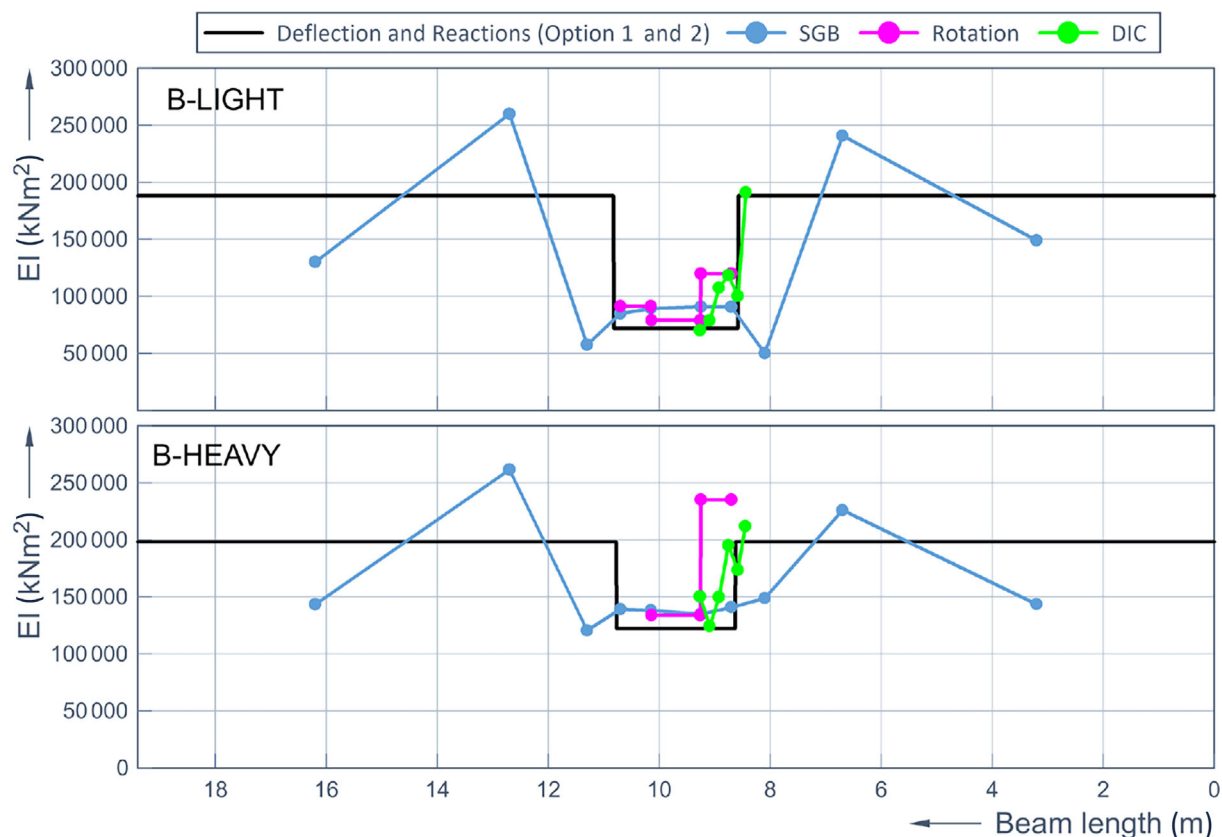
FIGURE 10 Bending stiffness *EI* for tested beams according to parallel measurements at load level $F_{tot} = 900$ kN.

The curvature κ can be calculated according to the tension steel strain ε_s, concrete strain in the extreme fiber ε_c and effective height d. The curvature is then,

$$\kappa = \frac{\varepsilon_c + \varepsilon_s}{d}. \tag{9}$$

At the hogging moment area, longitudinal tension steel is spread in the flange overhangs. When the studied section is located at the hogging moment area, ε_s is defined as an average value of four measuring points located in the deck. ε_c is determined according to one SGB located at the compression side.

EI(x) according to rotation measurements

Rotation in measuring lines 4–7 was measured during loading. Two rotation measuring lines were located on both sides of the center support. When the rotation of two vertical lines is known, the curvature between the measured lines can be calculated.

$$\kappa = \frac{\theta_1 + \theta_2}{e} \tag{10}$$

where, e = the horizontal distance between vertical measuring lines.

With the help of rotation measurements, three average bending stiffnesses could be determined between four measuring lines. An average bending moment value between the measuring lines has been used. At testing stage of B-HEAVY, rotation of measuring line 7 failed, as it yielded almost nonexistent rotation during the first stages of loading. Because of this, these measurements of the beam are not presented in the Figure 10.

EI(x) according to digital image correlation

Exactly, 170-mm-long extensometers (see Figure 11) were used both at the top e0...e4 and bottom e5...e9 parts of the beam web. The length and location of the extensometers were selected so that at least one tension crack formed in the measurement range of each top extensometer. With the help of these measurements and Equations 2 and 9 the curvature and bending stiffness could be determined at five points between in a distance of 8.6 and 9.3 m from the end support.

The uncertainty of DIC measurements is related to environmental variables influencing recordings produced via DIC, such as changing light, air conditioning, the temperature conditions, or a deterioration of the imaging performance in the edge areas of an image.[33]
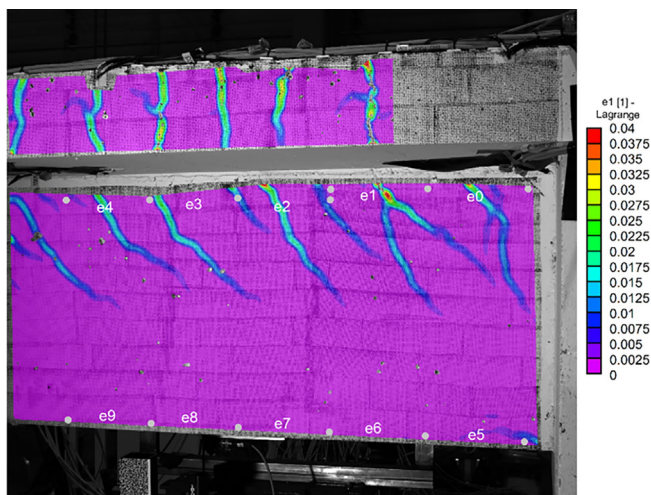
FIGURE 11 Principal tension strain and cracking of the B-HEAVY central support area according to the DIC technique at load level of $F_{tot} = 1850$ kN (xx% of failure load). The extensometer locations used are also presented.

4 | MODELING OF TESTED STRUCTURES

4.1 | Moment–curvature relationship

The variation of bending stiffness EI along the beam length can be determined on the basis of moment–curvature relations. The theoretical and measured $M-\kappa$ curves of the tested cross-sections are displayed in Sections 4.1.1 and 4.1.2.

During loading tests, it was observed that the cross-beam transferring compression between the prefabricated beams remained undamaged, and the failure always took place outside the diaphragm. Due to that, the following center support analysis is made for the T-shaped composite cross-section where the failure occurred. The test results presented from the support are also outside the diaphragm. An analysis of the diaphragm is beyond the scope of this study.

4.1.1 | Theoretical moment–curvature

The bending capacity of the studied structure is affected in SLS by tension stiffening and in ULS by confinement.[27,34] For these reasons, multiple material models needs to be considered in order to determine sufficiently accurate moment–curvature relation.

In this study, $M-\kappa$ for tested cross-sections have been determined with four different calculation METHODS, 1–4. Each METHOD contains different material model combinations, with each of them being suitable for the

cross-section and load level combination in question. The material models used for the METHODS 1–4 are presented in Figures 12–14. The combinations of used material models in the different methods are summarized in the Table 4.

Theorical $M-\kappa$ for inner support is determined in two phases. METHOD 1 is used before any yielding and METHOD 2 near failure. At inner support, the hogging moment is restricted by conventional reinforcing bars at the deck slab and tensile resistance of slab concrete has an effect on the pre- and postcracking behavior of the structure. The influence of tension stiffening, in the deck slab is considered in the material model of reinforcing steel which is considered in METHOD 1. The relation presented in Figure 14 is based on a simplified load–strain relation for a centrally reinforced member subjected to tension presented in the Reference 15. The effective area of concrete in tension is assumed to be the whole tensioned deck slab.

METHOD 2 is used at inner support for $M-\kappa$ relation near failure. Data from previous research has established that confinement has a remarkable role on the behavior of tested connections near failure.[27] Tightly spaced stirrups create confinement to the cross-section core and increase the ductility and capacity of the compressed soffit at the hogging moment area. Because of this, the confined concrete material model presented in Figure 12a is used for the analysis of precast prestressed beam near failure in the METHOD 2. The confining pressure from transverse stirrups for the concrete core was 1.7 MPa. The effect of prestress force in the compression side at the hogging moment area is taken into account at the analysis of center support according to the principal component analysis method presented in References 1,27.

Theorical $M-\kappa$ for prestressed composite beam in the span is determined with two parallel METHODS. METHOD 3 does not consider the effect of tension stiffening, whereas METHOD 4 considers tension stiffening in the tensile stress–strain model of the precast beam concrete according to Figure 12b.[34] The SLS behavior of the studied structure is effected by prestress losses. The ages of the precast beams were 37–44 days before the loading test. In order to determine the prestress losses caused by creep, shrinkage, and relaxation before that, the EC2 annex B approach was obtained.[11] Time-dependent losses were estimated to be 11% of the prestress launching force. The $M-\kappa$ relations are almost similar for METHODS 3 and 4. This finding is consistent with observations made by Lee (2022), who stated that "concrete members with higher prestressing force may be less affected (almost negligible) by concrete tension stiffening."[34] Theoretical $M-\kappa$ relations are presented for inner support and the span separately in Figures 15 and 16.
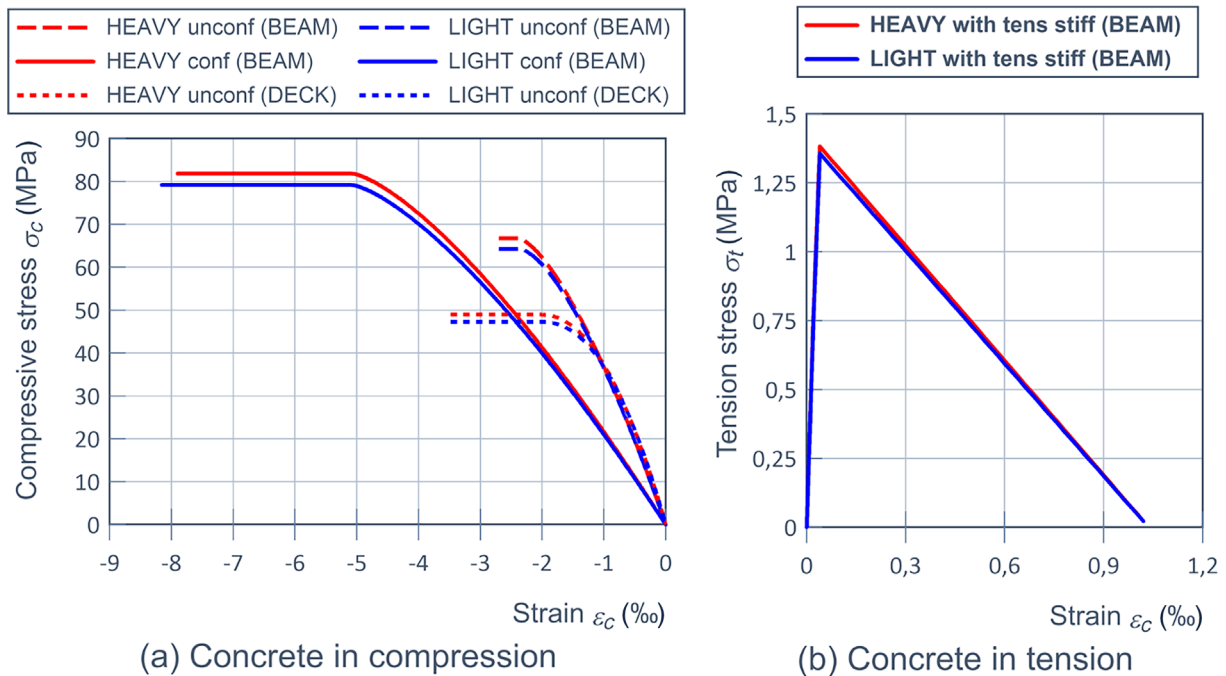
FIGURE 12   Concrete material models. (a) Compressive material models for deck slab and for confined and unconfined precast beam. (b) Tensile response of precast beam concrete considering tension stiffening.
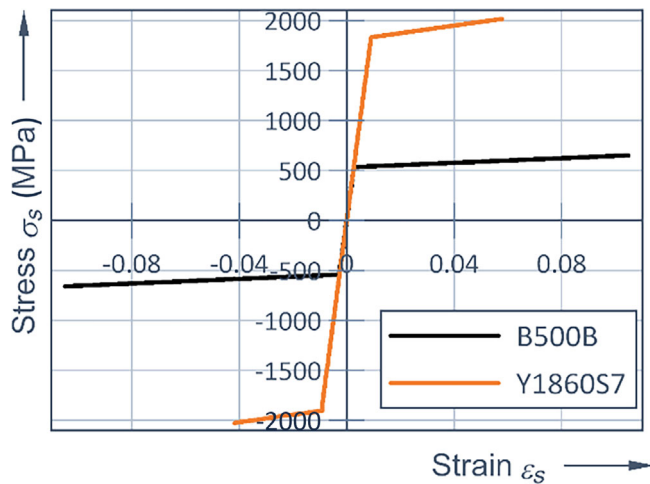

FIGURE 13   Stress–strain relation of steel bars B500B and prestressed strands Y1860S7 based on material testing. Effect of concrete is not considered.
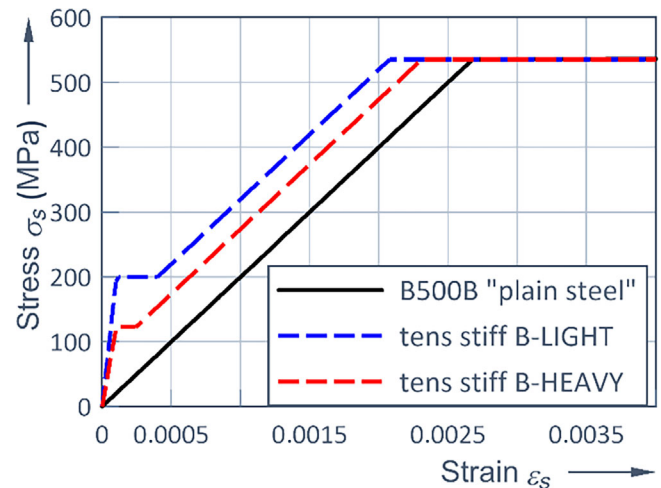

FIGURE 14   Stress–strain relation for centric deck reinforcement considering tension stiffening. For comparison, "plain" B500B steel determined first in Figure 13 is also presented in black.

4.1.2 | Moment–curvature according to test results

The curvature of eight critical sections was determined as the load was increased to failure from Equation (9) on the basis of SGB measurements. Figures 15 and 16 present experimental moment–curvature relations of the span and intermediate support of both tests based on SGB measurements. The SGBs remained functional in all tests at a load level of 96%–99% of failure load. The

moment values presented in Figures 15 and 16 are calculated based on measured support reactions and loads. The shift of the bending moment distribution at ULS caused by shear force is not considered. The width of the support is assumed to be 450 mm. The support reactions of the test beams were measured with load cells as the beams were laid down on the supports. With the help of this measured data the moment caused by self-weight, including possible restraint forces caused by the creep and differential shrinkage of the test beams, could be

TABLE 4   Material stress–strain relations used in METHODS 1–4.

	METHOD 1	METHOD 2	METHOD 3	METHOD 4
Concrete compression: Figure 12a unconfined BEAM (EC2 3.1.7)[11]	×		×	×
Concrete compression: Figure 12a confined BEAM (MC 2010 7.2.3.1.6)[15]		×		
Concrete compression: Figure 12a unconfined DECK (EC2 3.1.7)[11]	×	×	×	×
Concrete tension: zero for BEAM and DECK	×	×	×	
Concrete tension: zero for DECK and tensile response acc. (Figure 12b for BEAM)[34]				×
B500B: idealized stress–strain model Figure 13		×	×	×
B500B: stress–strain model considering tension stiffening Figure 14 (MC 2010 7.6-2)[15]	×			
Y1860S7: idealized stress–strain model Figure 13[15]	×	×	×	×
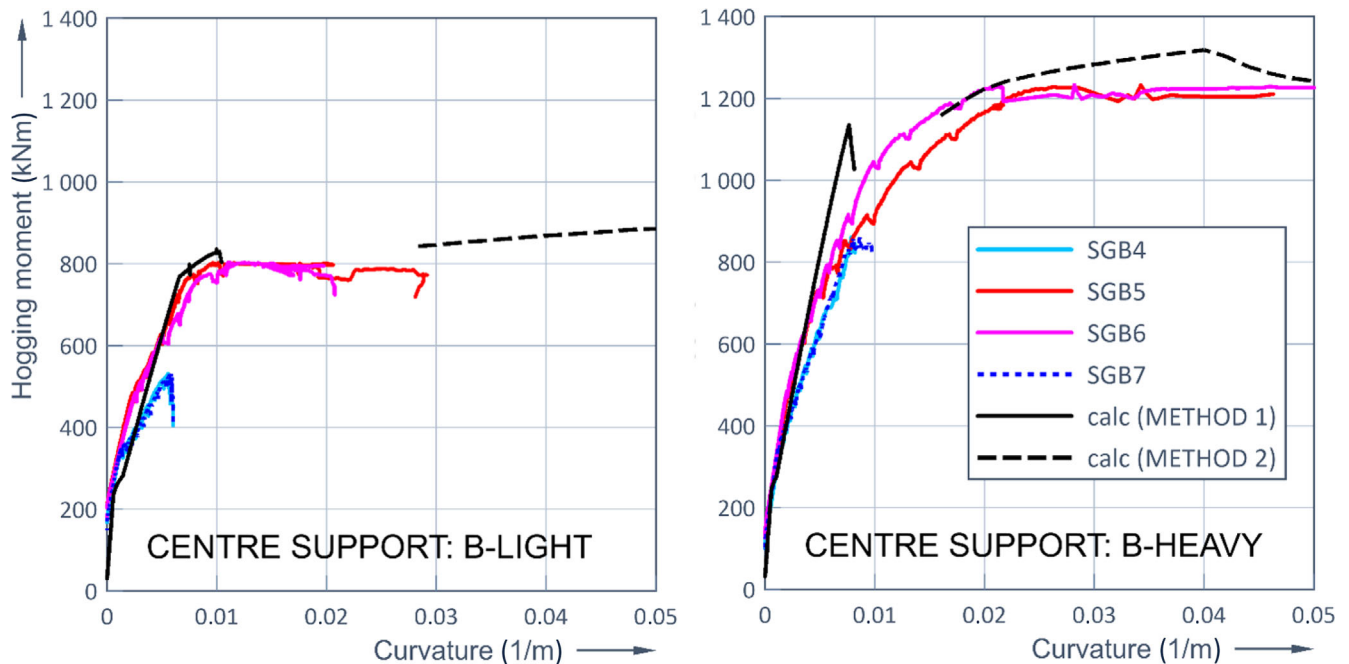
FIGURE 15   Experimental and theoretical $M-\kappa$ responses at the center support of the tested beams.

determined. These moment values are considered in Figures 15 and 16. It was not possible to measure the curvature of the test beams, as they were laid down on the supports. Because of that, the curvature caused by the self-weight of the beam is not included. The theoretical and tested $M-\kappa$ relations align well with each other.

4.2 | Comparison of calculated and experimental bending stiffness

The value of bending stiffness for a beam may be determined according to Equation (2). The tested and

calculated variations of the bending stiffness with bending moment are shown in Figures 17a,b and 18a,b. Curves 17a and 18a show the tested stiffness of both test beams at eight different locations according to the SGB measurements in the last loading cycle. The theoretical relations calculated according to METHODS 1 (for support) and 4 (for span) are presented in the (b) curves.

The comparison of Figures 17a,b and 18a,b reveals a considerable difference between the tested and calculated bending stiffness values. The tested uncracked bending stiffness of the span cross-section is only 61%–64% of the calculated value, and the same trend continues at the cracked stage. At the support area, the tested bending
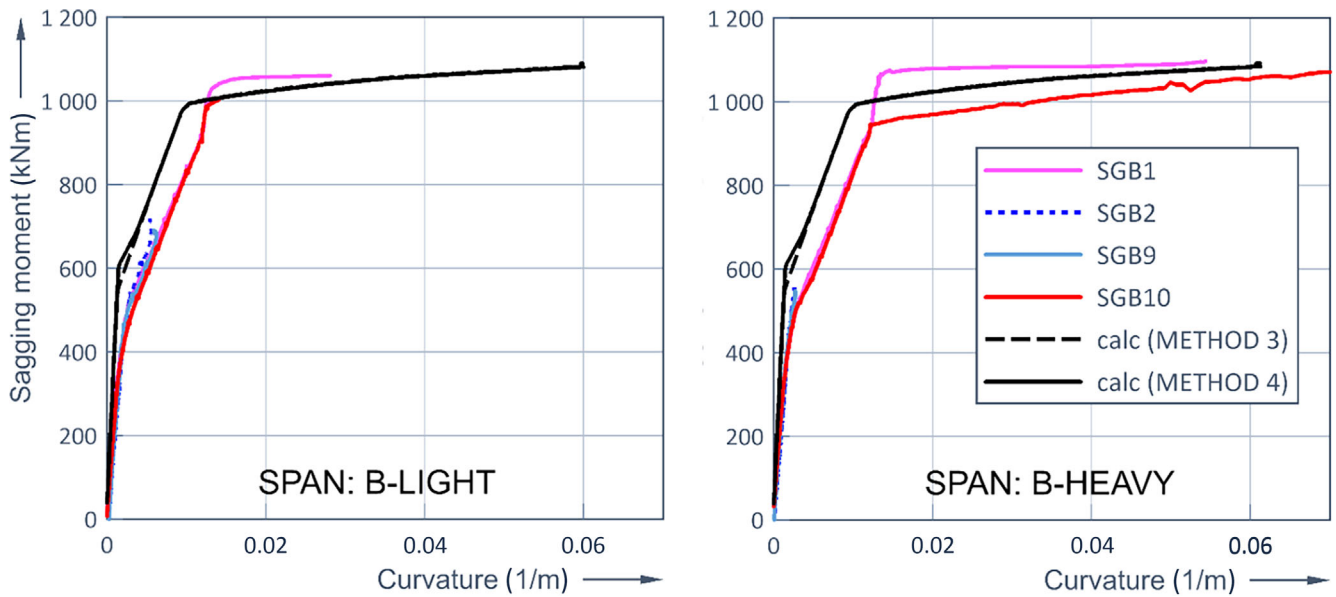
FIGURE 16   Experimental and theoretical $M - \kappa$ responses at the span of the tested beams.
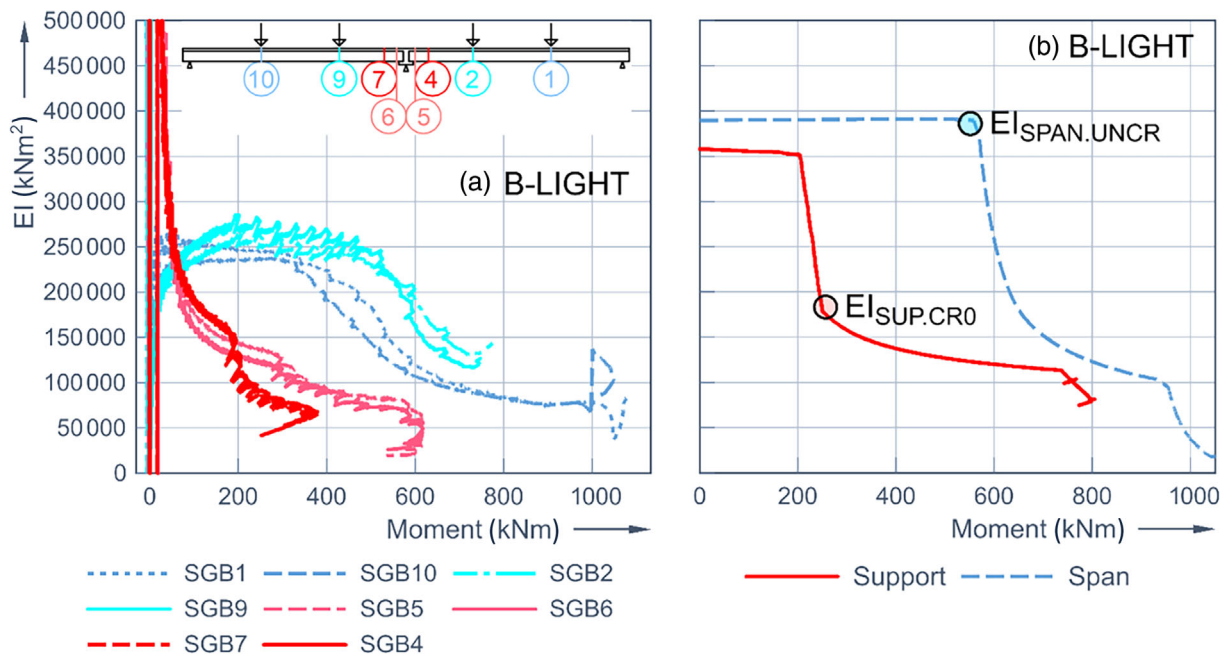

FIGURE 17   Bending stiffness of the B-LIGHT—Moment curve according to the strain gauge bar test results (a) and theoretical analysis (METHODs 1 and 4) (b).

stiffness does not show any sign of an uncracked stage. This result is explained by the fact that the support area of the test beam was cracked already at the first SLS tests that were made before loading to failure. When comparing completely cracked bending stiffness values next to the support, the tested stiffnesses are about 59%–64% of the calculated values. These results support previous research, which has found that it may be unreliable to predict the HSC modulus of elasticity from its compressive strength.[35–38] Although the values of the tested and

calculated bending stiffnesses are dissimilar, the shape of the relation curve between stiffness and bending moment is similar in them.

4.3 | Nonlinear analysis of the test beams

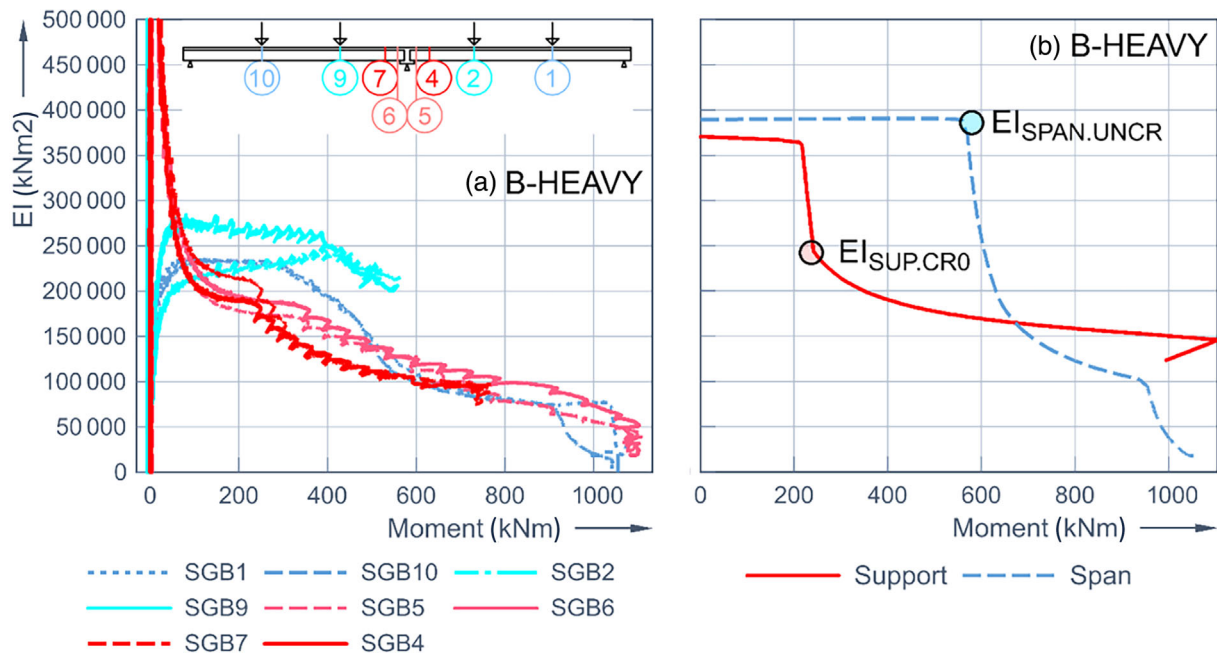As has been presented in the preceding sections the stiffness distribution of the studied structure changes from

FIGURE 18 Bending stiffness for the B-HEAVY—Moment curve according to the strain gauge bar test results (a) and theoretical analysis (METHODs 1 and 4) (b).
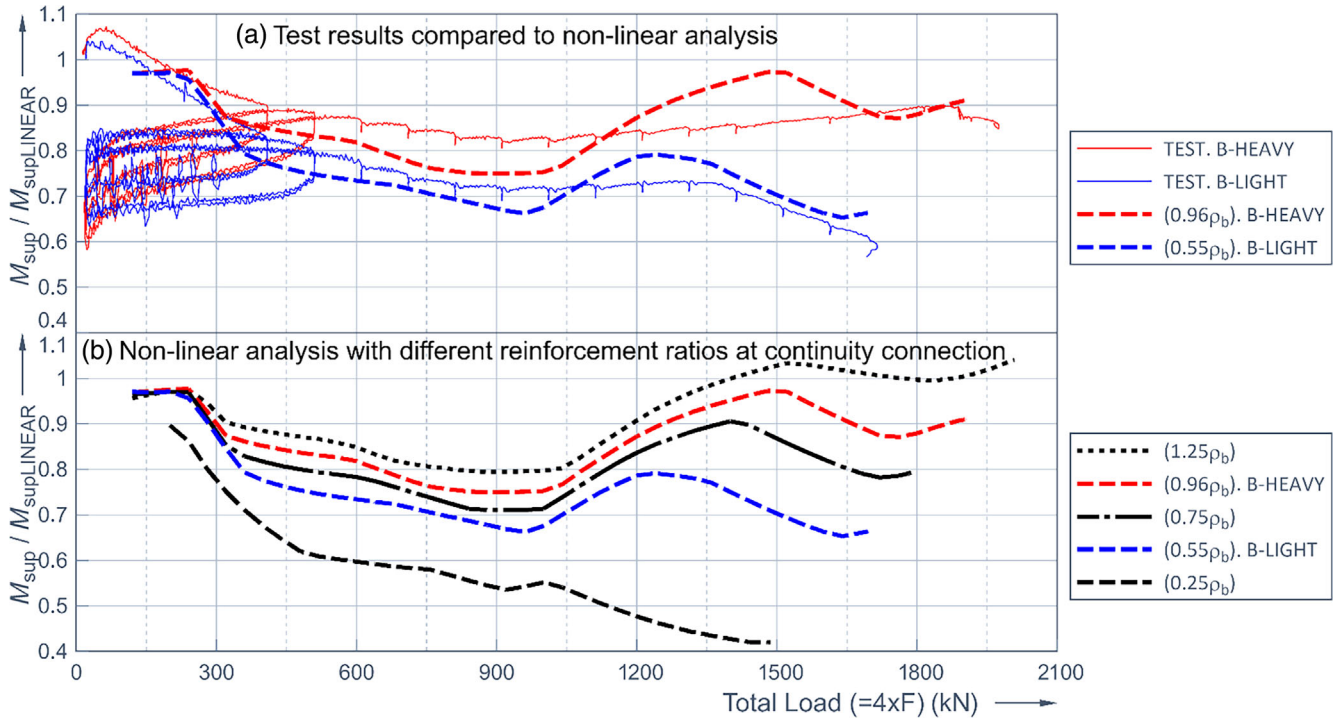

FIGURE 19 The variation of the ratio (Support bending moment $= M_{sup}$)/(Calculated support moment according to linear elastic analysis and the assumption that the stiffness of the girder is constant $= M_{supLINER}$) with an increase in total load according to the tests and nonlinear analysis.

the service to the ultimate strength state. A nonlinear analysis of the moment redistribution during loading was made to evaluate this observation theoretically. In the analysis, the support reactions of the studied beam were

solved with the help of the $M - \kappa$ relationship and unit force method. Besides tested cross-section properties nonlinear analysis was conducted also for three additional beams to cover the situations that were not

experimentally tested. The reinforcement ratio at the continuity connection in these analyses were $0.25\rho_b$, $0.75\rho_b$, and $1.25\rho_b$.

The theoretical nonlinear $M-\kappa$ behavior of tested cross-sections for sagging and hogging moment is determined in Section 4.1.1. The $M-\kappa$ models with METHODS 1, 2, and 4 considering tension stiffening and confinement were combined in a curvature range -6% to $+4\%$ and used in the nonlinear analysis. The continuous test beam was divided into 20 (0.3–3.2 m long) elements, and a simple nonlinear two-dimensional analysis was made. The length of the elements was shortened near the peak moments. The same $M-\kappa$ relation was used for every element, and the bending moment was assumed as constant at the length of the elements. The width of the support area was assumed to be 450 mm.

The comparison of nonlinear analyses and test results of moment redistribution is presented in Figure 19a. It is apparent from this figure that nonlinear analysis also predicts the early moment redistribution at the service state that was detected in the experimental tests. Parametric study made with nonlinear analysis and different reinforcement ratios at intermediate support are shown in Figure 19b. This analysis indicates that elastic redistribution as much as 20% will occur even though the beam is designed for zero redistribution at failure and reinforcement ratio at continuity connection is high ($1.25\rho_b$). Elastic redistribution achieved a value of over 40% in the

TABLE 5 Reduced bending stiffness values of the test beams at hogging moment area with different reinforcement ratios.

Reinforcement ratio	$EI_{SUP.CR0}$ (MNm²)	$K = \dfrac{EI_{SUP.CR0}}{EI_{SPAN.UNCR}}$
$0.25\rho_b$	112	0.29
$0.55\rho_b$, B-LIGHT	177	0.46
$0.75\rho_b$	213	0.55
$0.96\rho_b$, B-HEAVY	243	0.62
$1.25\rho_b$	278	0.71

Note: Blue refers to B-LIGHT and red to B-HEAVY.

nonlinear analysis for beam with low continuity reinforcement level ($0.25\rho_b$).

4.4 | Idealization of the structure in analysis

Nonlinear analysis is one alternative to predict the distribution; however, in the practical design phase linear methods are superior compared to nonlinear analysis due to their simplicity.

Few simplified idealizations for predicting moment redistribution in precast prestressed beams made continuous have been presented in the literature. Oesterle (1989) suggested that in case the hogging moment at intermediate support exceeds 125% of its cracking moment, the midspan moment should be taken as the resultant sagging moment from continuous analysis in addition to the amount by which the negative continuity moment exceeds 125% of the cracking moment.[7] The other approach was made by Clark and Sugie who proposed that at the service limit state the hogging moment could be reduced by 10% of the value calculated according to the uncracked stiffnesses.[39] Moment redistribution achieved with these approaches is presented in Figure 21 with the label Idealization, NCHRP[7] and Clark and Sugie.[39]

To address this question from another direction, a new idealization of the structural model for the elastic analysis is presented here. Idealization is based on the test results presented in the previous sections. In this proposed idealization for the structural model, the girder's span area is assumed to stay uncracked and corresponding stiffness $EI_{SPAN.UNCR}$ is used. Contrary to that, the stiffness of the support area is assumed to be the cracked bending stiffness of the cross-section $EI_{SUP.CR0}$, just after the first cracks have opened. The methods to determine these stiffness values are presented in Section 4.2 and the values are also highlighted at Figures 17b and 18b. Table 5 below presents the summary of reduced bending stiffness values at the
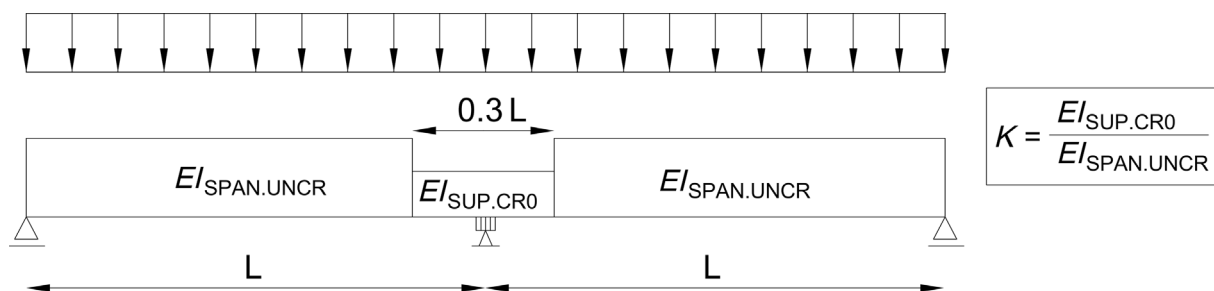

FIGURE 20 Definition of simplified stiffness distribution of precast prestressed beam made continuous at the load stage where hogging moment at support exceeds the negative cracking moment.
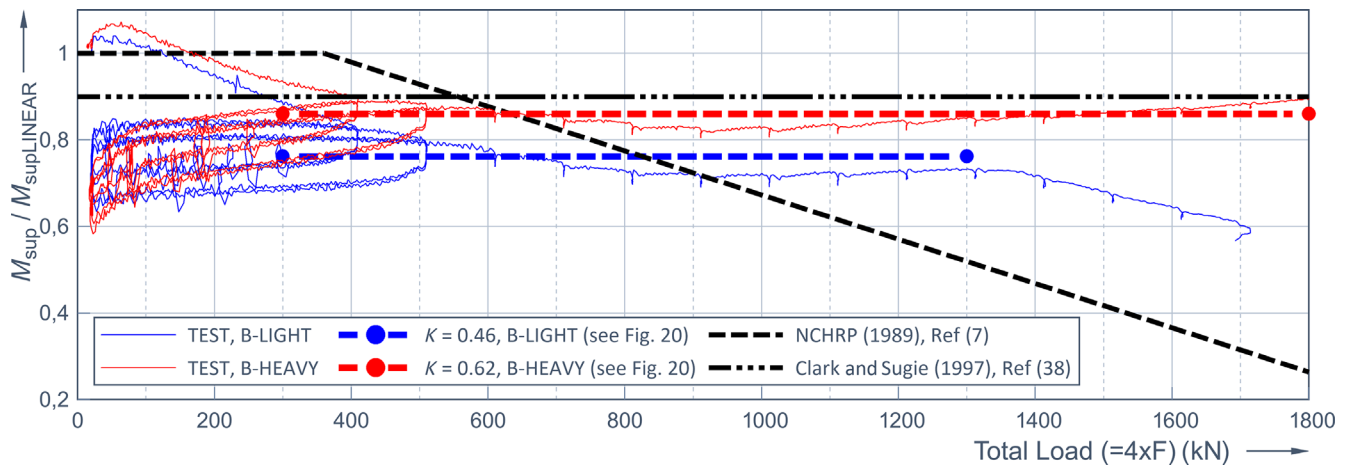
FIGURE 21 The variation of ratio $M_{sup}/M_{supLINEAR}$ with increase in total load accordingly simplified idealizations compared to test results.

hogging moment area of the beams that were nonlinearly analyzed in the previous section.

The length of the softened support area depends on the length of the hogging moment area. In the Reference 11, the definition of the relevant distance of the hogging area in the continuous concrete beam, when defining the effective width of the flanges, is assumed to be 0.3 L.[11,15] This same approach was adopted here. The definition of the simplified stiffness model is presented in Figure 20 and the results of the simplified idealizations are compared to the experimental results in the Figure 21. Whereas the method presented by NCHRP and Clark and Sugie does not depend on the reinforcement amount of the deck slab at the connection idealization presented in this article determines the service state bending stiffness of the support area according to case-specific moment–curvature relation and as a result the amount of tension reinforcement has an effect.

5 | CONCLUSIONS

The purpose of this study was to investigate the moment redistribution of precast prestressed beams made continuous. Based on the data and results presented in this article, the following conclusions can be made:

1. During loading tests, remarkable moment redistribution (14%–44%) was detected and the observed moments in the structure were significantly different compared to the moments predicted with uncracked constant bending stiffness distribution.
2. Cracking of the concrete is traditionally assumed to have a minor effect on the global behavior of the studied intermediate structure.[9] Experimental results of this study however indicate that cracking is in vital role for the occurrence of observed moment redistribution. The measured bending stiffness of the intermediate support region was considerably smaller than that of the midspan regions already at early stage of load process, which lead to elastic redistribution. The relative magnitude of this elastic redistribution was significant in the studied structure (65%–100%). If elastic redistribution is neglected in the structural analysis, the service state sagging moment at the midspan of the beam may end up in the unconservative side.
3. Parametric nonlinear study made for different continuity reinforcement levels indicates that elastic redistribution is considerable in the studied structure although beams have been designed for zero redistribution at ULS. As a consequence the beam with high reinforcement levels at hogging moment area undergoes reverse plastic redistribution before failure.
4. Taken together, the experimental results suggest that the relation of the bending stiffnesses between intermediate support and span is nearly constant after cracking of the connection up to the yielding point. The length of the reduced stiffness at intermediate support increases, but after the increase has reached a certain value it does not have a significant effect on moment distribution because of the vicinity of the point of contraflexure. Due to this, a simplified idealization for design may have been proposed.
5. Since the study was limited to evaluate the bending stiffness distribution and its effect on the moment redistribution, it was not possible to also include the consideration of crack widths in this study. A decrease in the stiffness indicates extensive cracking, which limits the application of the studied structure. This would be an important area for further research.

6. Although the test samples were large, they were not full-sized and the amount of them was limited, which is a limitation of this study. In real structure, the deck slab may be considerably wider compared to the test specimen. An issue that was not addressed in this study is how high effect the scaled deck slab width has into the conclusions of this study.

DATA AVAILABILITY STATEMENT
The data that support the findings of this study are available from the corresponding author upon reasonable request.

ORCID
Ulla Kytölä https://orcid.org/0000-0003-0645-8146
Joonas Tulonen https://orcid.org/0000-0002-0879-244X
Olli Asp https://orcid.org/0000-0003-4022-8336
Anssi Laaksonen https://orcid.org/0000-0001-8459-7470

REFERENCES
1. Kaar PH, Kriz LB, Hognestad E. Precast-prestressed concrete bridges 1. Pilot tests of continuous girders. J PCA Res Dev Lab. 1960;2:21–37.
2. Newhouse CD, Roberts-Wollmann CL, Cousins TE. Development of an optimized continuity diaphragm for new PCBT girders; 2005.
3. Freyermuth CL. Design of Continuous Highway Bridges with precast, prestressed concrete girders. PCI J. 1969;14:14–39.
4. Ibrahim MS, Yang Y, Roosen M, Hendriks MAN. Challenges on the shear behavior of existing continuous precast girder bridges. Proc 14th Fib Int PhD Symp Civil Eng; 2022.
5. Mattock AH. Precast-prestressed concrete bridges 5. Creep and shrinkage studies. J PCA Res Dev Lab. 1961;2:32–66.
6. McDonagh MD, Hinkley KB. Resolving restraint moments: designing for continuity in precast prestressed concrete girder bridges. PCI J. 2003;48(4):104–19. https://doi.org/10.1016/j.physb.2007.02.012
7. Oesterle RG, Glikin JD, Larson SC. Design of precast, prestressed bridge girders made continuous. Transportation Research Board, National Research Council; 1989.
8. Mirmiran A, Kulkarni S, Castrodale R, Miller R, Hastak M. Nonlinear continuity analysis of precast, prestressed concrete girders with cast-in-place decks and diaphragms. PCI J. 2001;46(5):60–80. https://doi.org/10.15554/pcij.09012001.60.80
9. AASHTO. AASHTO LRFD bridge design specifications; 2012.
10. Menkulasi F, Patel A, Baghi H. An investigation of AASHTO's requirements for providing continuity in simple span bridges made continuous. Eng Struct. 2018 Mar;158:175–98. https://doi.org/10.1016/j.engstruct.2017.12.019
11. EN 1992-1-1. Eurocode 2: Design of concrete structures. Part 1-1: General rules and rules for buildings; 2005.
12. E. 1992-2. Eurocode 2: Design of concrete structures. Part 2: Concrete bridges. Design and detailing rules; 2005.
13. Hendy CR, Smith DA. Designers' guide to EN 1992–2, Eurocode 2:design of concrete structures. Part 2: Concrete bridges. London: Thomas Telford Publisihing; 2007.
14. Li L, Zheng W, Wang Y. Review of moment redistribution in statically indeterminate RC members. Eng Struct. 2019;196:109306. https://doi.org/10.1016/j.engstruct.2019.109306
15. FIB. Fib Bulletin 66, Model Code 2010, Final draft, Volume 2. Lausanne, Switzerland: International Federation for Structural Concrete (fib); 2012.
16. Li L, Li B, Guo N, Zheng W. Experimental and numerical investigations on moment redistribution in reinforced concrete frames subjected to vertical loads. Eng Struct. 2022;261:114289. https://doi.org/10.1016/j.engstruct.2022.114289
17. Leung CCY, Au FTK, Kwan AKH. Non-linear analysis and moment redistribution of prestressed concrete members. Eng Comp Mech. 2013;166(1):9–21. https://doi.org/10.1680/eacm.11.00021
18. Lou T, Liu M, Lopes SMR, Lopes AV. Moment redistribution in two-span prestressed NSC and HSC beams. Mater Struct. 2017 Dec;50(6):246. https://doi.org/10.1617/s11527-017-1116-5
19. Kodur VKR, Campbell TI. Evaluation of moment redistribution in a two-span continuous prestressed concrete beam. ACI Struct J. 1996;93(6):721–8. Nov.
20. Kodur VKR. Factors governing redistribution of moment in continuous prestressed concrete beams. Struct Eng Mech. 1999;8(2):119–36. https://publications-cnrc.canada.ca/fra/droits
21. Scott RH, Whittle RT. Moment redistribution effects in beams. Mag Concr Res. 2005 Feb;57(1):9–20. https://doi.org/10.1680/macr.57.1.9.57870
22. Mattock AH. Redistribution of design bending moments in reinforced concrete continuous beams. Proc Inst Civ Eng. 1959;13(1):35–46.
23. Berger J. Effects of flexural stiffness on constraints of imposed deformations in reinforced concrete structures. Eng Struct. 2022;272:1–8. https://doi.org/10.1016/j.engstruct.2022.114973
24. Bagge N, O'Connor A, Elfgren L, Pedersen C. Moment redistribution in RC beams—a study of the influence of longitudinal and transverse reinforcement ratios and concrete strength. Eng Struct. 2014;80:11–23. https://doi.org/10.1016/j.engstruct.2014.08.029
25. Lopes SMR, Harrop J, Gamble AE. Study of moment redistribution in prestressed concrete beams. J Struct Eng. 1997;123(5):561–6. https://doi.org/10.1061/(ASCE)0733-9445(1999)125:3(351)
26. Hegger G. Stahlbetonbau aktuell 2013. Praxishandbuch.
27. Kytölä U, Asp O, Laaksonen A. Negative bending tests on precast prestressed concrete beams made continuous. Struct Concr. 2021;22(4):2223–42. https://doi.org/10.1002/suco.202100043
28. EN. Eurocode: basis of structural design; 2002. 1990.
29. Mattock AH, Kaar PH. Precast-prestressed concrete bridges 3. Further tests of continuous girders. J PCA Res Dev Lab. 1960;2:51–78.

30. Derucher K, Putcha C, Kim U. Indeterminate structural analysis. Lewiston, NY: The Edwin Mellen Press, Ltd; 2013.

31. Gere J, Timoshenko S. Mechanics of materials; 1984.

32. Salmi T, Kuula K. Rakenteiden Mekaniikka; 2017.

33. Clauß F, Ahrens MA, Mark P. A comparative evaluation of strain measurement techniques in reinforced concrete structures—a discussion of assembly, application, and accuracy. Struct Concr. 2021 Oct;22(5):2992–3007. https://doi.org/10.1002/suco.202000706

34. Dong Lee J. The effect of tension stiffening in moment-curvature responses of prestressed concrete members. Eng Struct. 2022;257:114043. https://doi.org/10.1016/j.engstruct.2022.114043

35. Kytölä U, Laaksonen A. Prediction of restraint moments in precast prestressed structures made continuous. Nord Concr Res. 2018;2:73–93.

36. Shannag MJ. High strength concrete containing natural pozzolan and silica fume. Cem Concr Compos. 2000;22:399–406.

37. Noguchi T, Tomosawa F, Nemati KM, Chiaia BM, Fantilli AR. A practical equation for elastic modulus of concrete. ACI Struct J. 2009;106(5):690–6. https://doi.org/10.14359/51663109

38. Baalbaki W, Aitcin PC, Ballivy G. On predicting modulus of elasticity in high-strength concrete. ACI Mater J. 1992;89:517–20.

39. Clark LA, Sugie I. Serviceability limit state aspects of continuous bridges using precast concrete beams. Struct Eng. 1997;75(11):185–90.

AUTHOR BIOGRAPHIES

Ulla Kytölä, PhD student, Faculty of Built Environment—Concrete and Bridge Structures, Tampere University, Tampere, Finland. ulla.kytola@tuni.fi

Joonas Tulonen, PhD student, Faculty of Built Environment—Concrete and Bridge Structures, Tampere University, Tampere, Finland. joonas.tulonen@tuni.fi

Olli Asp, PhD student, Faculty of Built Environment—Concrete and Bridge Structures, Tampere University, Tampere, Finland. olli.asp@tuni.fi

Tarja Nakari, PhD student, Faculty of Built Environment—Concrete and Bridge Structures, Tampere University, Tampere, Finland. tarja.nakari@tuni.fi

Anssi Laaksonen, Professor, Faculty of Built Environment—Concrete and Bridge Structures, Tampere University, Tampere, Finland. anssi.laaksonen@tuni.fi